LETTER

doi:10.1038/nature10923

Trans-synaptic Teneurin signalling in neuromuscular synapse organization and target choice

Timothy J. Mosca[1]*, Weizhe Hong[1]*, Vardhan S. Dani[1], Vincenzo Favaloro[1] & Liqun Luo[1]

Synapse assembly requires trans-synaptic signals between the pre- and postsynapse[1], but our understanding of the essential organizational molecules involved in this process remains incomplete[2]. Teneurin proteins are conserved, epidermal growth factor (EGF)-repeat-containing transmembrane proteins with large extracellular domains[3]. Here we show that two *Drosophila* Teneurins, Ten-m and Ten-a, are required for neuromuscular synapse organization and target selection. Ten-a is presynaptic whereas Ten-m is mostly postsynaptic; neuronal Ten-a and muscle Ten-m form a complex *in vivo*. Pre- or postsynaptic Teneurin perturbations cause severe synapse loss and impair many facets of organization trans-synaptically and cell autonomously. These include defects in active zone apposition, release sites, membrane and vesicle organization, and synaptic transmission. Moreover, the presynaptic microtubule and postsynaptic spectrin cytoskeletons are severely disrupted, suggesting a mechanism whereby Teneurins organize the cytoskeleton, which in turn affects other aspects of synapse development. Supporting this, Ten-m physically interacts with α-Spectrin. Genetic analyses of *teneurin* and *neuroligin* reveal that they have differential roles that synergize to promote synapse assembly. Finally, at elevated endogenous levels, Ten-m regulates target selection between specific motor neurons and muscles. Our study identifies the Teneurins as a key bi-directional trans-synaptic signal involved in general synapse organization, and demonstrates that proteins such as these can also regulate target selection.

Vertebrate teneurins are enriched in the developing brain[4,5], localize to synapses in culture[6], and pattern visual connections[7]. Both *Drosophila* Teneurins, Ten-m and Ten-a, function in olfactory synaptic partner matching[8] and were further identified in neuromuscular junction (NMJ) defect screens[9,10], with Ten-m also affecting motor axon guidance[11]. We examine their roles and the underlying mechanisms involved in synapse development.

Both Ten-m and Ten-a were enriched at the larval NMJ (Fig. 1a and Supplementary Fig. 1a). Ten-a was detected at neuronal membranes: this staining was undetectable beyond background in *ten-a* null mutants (Supplementary Fig. 1b) and barely detectable after neuronal *ten-a* RNA interference (RNAi; Supplementary Fig. 1c), indicating that Ten-a is predominantly presynaptic. Partial co-localization was observed between Ten-a and the periactive zone marker Fasciclin 2 (ref. 12) as well as the active zone marker Bruchpilot[13] (Fig. 1b, c), suggesting that Ten-a is localized to the junction between the periactive zone and the active zone. Ten-m appeared strongly postsynaptic and surrounded each bouton (Fig. 1a and Supplementary Fig. 1a, d). Muscle-specific *ten-m* RNAi eliminated the postsynaptic staining, but uncovered weak presynaptic staining (Supplementary Fig. 1e) that ubiquitous *ten-m* RNAi eliminated (Supplementary Fig. 1f). Thus, the Ten-m signal was specific and, although partly presynaptic, enriched postsynaptically. Consistently, muscle Ten-m colocalized extensively with Dlg (Fig. 1d) and completely with α-Spectrin (Fig. 1e) and is thus probably coincident with all postsynaptic membranes.

The localization of Ten-a and Ten-m suggested their trans-synaptic interaction. To examine this, we co-expressed Myc-tagged Ten-a in nerves using the Q system[14] and haemagglutinin (HA)-tagged Ten-m in muscles using GAL4. Muscle Ten-m was able to co-immunoprecipitate nerve Ten-a from larval synaptosomes (Fig. 1f), suggesting that the Teneurins form a heterophilic trans-synaptic receptor pair at the NMJ.

To determine Teneurin function at the NMJ, we examined the *ten-a* null allele and larvae with neuron or muscle RNAi of *ten-a* and/or *ten-m*. Following such perturbations, bouton number and size were altered: the quantity was reduced by 55% (Fig. 2a–c, g and Supplementary Fig. 2)

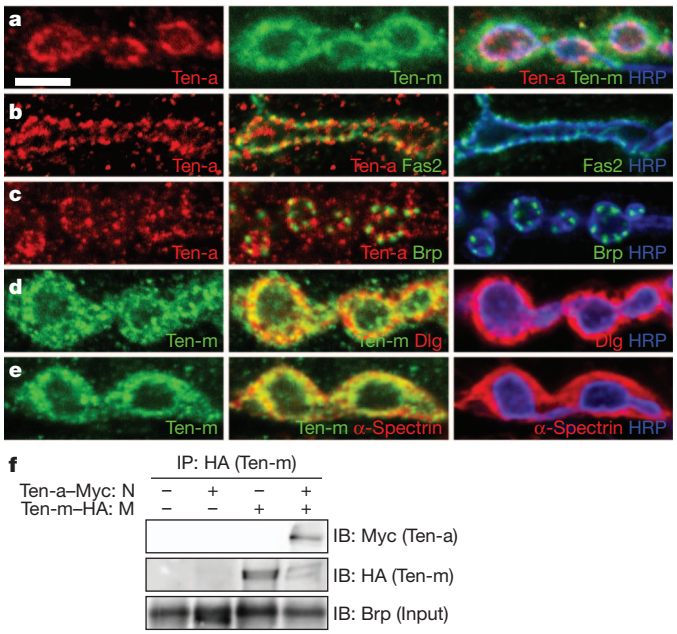

Figure 1 | Teneurins are enriched at and interact across *Drosophila* neuromuscular synapses. **a**–**e**, Representative single confocal sections of synaptic boutons stained with antibodies against Ten-a (red) or Ten-m (green), horseradish peroxidase (HRP) to mark the neuronal membrane (blue), and a synaptic marker as indicated. **a**, Ten-a is associated with presynaptic membranes and Ten-m largely with the surrounding postsynapse (**a**). **b**, **c**, Ten-a shows limited co-localization with the periactive zone marker Fasciclin 2 (**b**), and Bruchpilot (Brp), an active zone marker (**c**). **d**, **e**, Ten-m co-localizes with, and extends beyond, Dlg (**d**) and completely co-localizes with muscle α-Spectrin (**e**). **f**, Immunoblots (IB) of larval synaptosomes expressing neuronal Flag–Myc-tagged Ten-a (N) and muscle Flag–HA-tagged Ten-m (M) and immunoprecipitated (IP) using antibodies to HA. Ten-a is detected in the pull-down, indicating that nerve Ten-a and muscle Ten-m interact across the NMJ. This is not seen in control lanes. Owing to low expression, neither transgene product is detectable in input lysates, which are enriched in Brp. Scale bar, 5 μm.

[1]Department of Biology, Howard Hughes Medical Institute, Stanford University, Stanford, California 94305, USA.
*These authors contributed equally to this work.

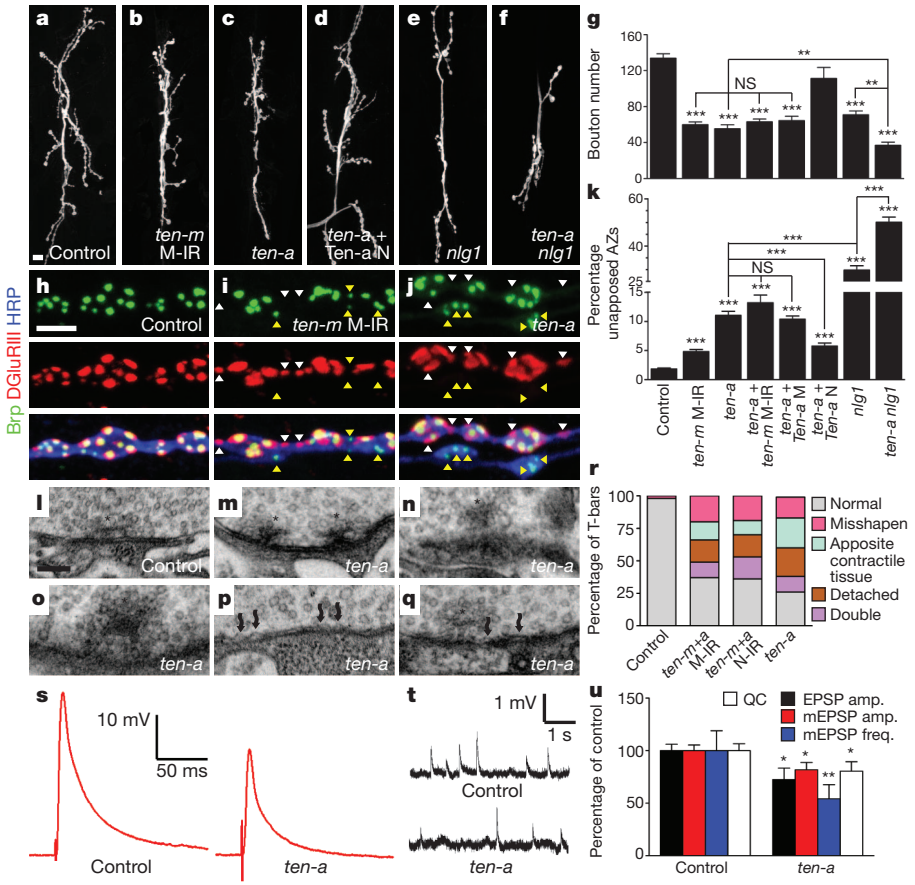

Figure 2 | Teneurins affect the structure and function of the neuromuscular synapse. **a**–**f**, Representative NMJs stained with antibodies to HRP. Muscle-specific *ten-m* RNAi (M-IR) and lots of *ten-a* decrease bouton number. Neuronal (Ten-a N) but not muscle (Ten-a M) restoration of *ten-a* expression rescues this phenotype. These defects resemble *nlg1* mutants and are enhanced in *ten-a nlg1* double mutants. **g**, Quantification of bouton number. **h**–**j**, Representative NMJs stained with antibodies to Brp (green), the glutamate receptor subunit DGluRIII (red) and HRP (blue). In control larvae (**h**), Brp and DGluRIII puncta properly appose. *teneurin* perturbations (**i**, **j**) disrupt this active zone (yellow arrowhead) and glutamate receptor apposition (white arrowhead). **k**, Quantification of unapposed active zone/glutamate receptor pairs. For each quantification, $n \geq 8$ larvae, 16 NMJs. **l**–**q**, Transmission electron microscopy of active zone T-bars (asterisks) in control larvae (**l**) and *ten-a* mutants (**m**–**q**) showing double T-bars (**m**), detached T-bars (**n**), misshapen T-bars (**o**), membrane ruffling (**p**, waved arrows) and T-bars facing contractile tissue (**q**). Some images show multiple defects. **r**, Distribution of T-bar defects as a percentage of the total T-bars. N-IR, neuronal RNAi. For each genotype, $n \geq 3$ larvae, 40 boutons. **s**, **t**, Representative evoked EPSP (**s**) and mEPSP (**t**) traces from control and *ten-a* mutant genotypes. **u**, Quantification of mean EPSP amplitude (black), mEPSP amplitude (red), mEPSP frequency (blue) and quantal content (QC, white) expressed as a percentage of the control average. For all genotypes, $n \geq 7$ larvae, 8 muscles. Error bars represent s.e.m. Scale bars, 10 μm (**a**–**f**), 5 μm (**h**–**j**), 100 nm (**l**–**q**). $***P < 0.001$, $**P < 0.01$, $*P < 0.05$, NS, not significant. Statistical comparisons are with control unless noted.

and the incidence of large boutons markedly increased (Supplementary Fig. 2k). Both changes indicate impaired synaptic morphogenesis. The reduction in bouton number was probably cumulative through development, as it was visible in first instar *ten-a* mutants and persisted (Supplementary Fig. 2k). In the *ten-a* mutant, bouton morphogenesis was rescued by restoring Ten-a expression in neurons, but not muscles (Fig. 2d, g and Supplementary Fig. 2). Neuronal Ten-m overexpression could not substitute for the lack of Ten-a, revealing their non-equivalence (Supplementary Fig. 2e, l). Neuronal knockdown of Ten-a or Ten-m resulted in fewer synaptic boutons (Supplementary Fig. 2f–h, l), indicating that both have a presynaptic function, although presynaptic Ten-a has a more predominant role (Supplementary Fig. 2l). Moreover, knocking down postsynaptic Ten-m in the *ten-a* mutant did not enhance the phenotype (Fig. 2g). Thus, presynaptic Ten-a (and, to a lesser extent, Ten-m) and postsynaptic Ten-m are required for synapse development.

teneurin perturbation also caused defects in the apposition between presynaptic active zones (release sites) and postsynaptic glutamate receptor clusters[15] (Fig. 2h and Supplementary Fig. 3): up to 15% of the active zones/receptor clusters lacked their partner compared to 1.8% in controls (Fig. 2h–k). Under electron microscopy, active zones are marked by electron-dense membranes and single presynaptic specializations called T-bars (Fig. 2l), which enable synapse assembly, vesicle release and Ca^{2+}-channel clustering[16]. Teneurin disruption caused defects (Fig. 2m–r and Supplementary Fig. 3) in T-bar ultrastructure (Fig. 2m–o), membrane organization, and apposition to contractile tissue (Fig. 2p, q). Teneurin perturbation also impaired postsynaptic densities while increasing membrane ruffling (Supplementary Table 1), further indicating organizational deficiency. These phenotypes resemble mutants with adhesion and T-bar biogenesis defects[17,18], suggesting a role for Teneurins in synaptic adhesion and stability. Synaptic vesicle populations similarly required Teneurins for clustering at the bouton perimeter and proper density (Supplementary Fig. 4). As these effects are not synonymous with active zone disruption[19], Teneurins are also required for synaptic vesicle organization.

Synapses lacking *teneurin* were also functionally impaired. The mean amplitude of evoked excitatory postsynaptic potentials (EPSPs) in larvae was decreased by 28% in the *ten-a* mutant (Fig. 2s, u). Spontaneous miniature EPSPs showed a 20% decrease in amplitude, a 46% decrease in frequency (Fig. 2t, u), and an altered amplitude distribution compared with control (Supplementary Fig. 5a). These defects resulted in a 20% reduction in quantal content (Fig. 2u), which could be partly due to

fewer boutons and release sites. However, release probability may also be reduced, as suggested by an increased paired pulse ratio in *ten-a* mutants (Supplementary Fig. 5d, e). The decay kinetics of responses were faster in *ten-a* mutants, suggesting additional postsynaptic effects on glutamate receptors and/or intrinsic membrane properties (Supplementary Fig. 5b, c). Further, FM1-43 dye loading revealed markedly defective vesicle cycling in *ten-a* mutants (Supplementary Fig. 5f, h). Consistent with physiological impairment, *teneurin*-perturbed larvae exhibited profound locomotor defects (Supplementary Fig. 5i). In summary, Teneurins are required for multiple aspects of NMJ organization and function.

As a potential mechanism for synaptic disorganization following *teneurin* perturbation, we examined the pre- and postsynaptic cytoskeletons. In the presynaptic terminal, organized microtubules contain Futsch (a microtubule-binding protein)-positive 'loops', whereas disorganized microtubules possess punctate, 'unbundled' Futsch[20]. Each classification normally represented ~10% (often distal) of boutons (Fig. 3a, d and Supplementary Fig. 6). Upon *teneurin* perturbation, many more boutons had unbundled Futsch (Fig. 3b, c and Supplementary Fig. 6) whereas those with looped microtubules were decreased by 62–95% (Fig. 3d). Therefore, proper microtubule organization requires pre- and postsynaptic Teneurins. In contrast to mild active zone/glutamate receptor apposition defects, most boutons displayed microtubule organizational defects.

teneurin perturbation also severely disrupted the postsynaptic spectrin cytoskeleton, with which Ten-m colocalized (Fig. 1e). Postsynaptic α-Spectrin normally surrounds the bouton (Fig. 3e). Perturbing neuronal or muscle Teneurins markedly reduced postsynaptic α-Spectrin without affecting Dlg (Fig. 3f–h and Supplementary Fig. 7). Postsynaptic β-Spectrin[21], Adducin[22] and Wsp were similarly affected (Supplementary Fig. 8). In muscle, α-Spectrin is coincident with and essential for the integrity of the membranous subsynaptic reticulum (SSR)[21,23]. Consistent with this, *teneurin* disruption reduced SSR width up to 70% (Supplementary Fig. 9d–g) and increased the frequency of 'ghost' boutons, which are failures of postsynaptic membrane organization[23] (Supplementary Fig. 9a–d). Thus, Teneurins are involved in the organization of the pre- and postsynaptic cytoskeletons and postsynaptic membranes. Further, endogenous α-Spectrin co-immunoprecipitated with muscle-expressed, Flag-tagged Ten-m (Fig. 3i), suggesting that Ten-m physically links the synaptic membrane to the cytoskeleton.

Because the most severe defects following *teneurin* perturbation were cytoskeletal, we propose that Teneurins primarily organize the presynaptic microtubule and postsynaptic spectrin-based cytoskeletons (Fig. 3j), which then organize additional synaptic aspects[20,21]. However, such a solitary role cannot fully explain the observed phenotypes. The reduction in bouton number associated with cytoskeletal disruption is milder than that following *teneurin* disruption[20,21,24]. Also, although active zone dynamics are affected by cytoskeletal perturbation[21], defects in apposition are not[21,25]. Moreover, the T-bar structural defects more closely resemble synapse adhesion and active zone formation defects[17,18]. Thus, Teneurins may regulate release site organization and synaptic adhesion independent of the cytoskeleton (Fig. 3j).

Our data also indicate that Teneurins act bi-directionally across the synaptic cleft. Ten-a acts predominantly in neurons, as evidenced by localization, phenotypes caused by neuronal (but not muscle) knockdown, and mutant rescue by neuronal (but not muscle) expression (Figs 2 and 3 and Supplementary Figs 2–4, 6, 7 and 9). Yet, in addition to the presynaptic phenotypes, many others were postsynaptic, including reduced muscle spectrin, SSR, and membrane apposition (Fig. 3 and Supplementary Figs 7–9). Similarly, although Ten-m is present both pre- and postsynaptically, muscle knockdown resulted in presynaptic defects, including microtubule and vesicle disorganization, reduced active zone apposition, and T-bar defects (Figs 2 and 3 and Supplementary Figs 3, 4, 6 and 7). Thus, Teneurins function in bi-directional trans-synaptic signalling to organize neuromuscular synapses. This may involve downstream pathways or simply establish an organizational framework by the receptors themselves. Moreover, as the results of single disruptions of neuronal *ten-a* or muscle *ten-m* were similarly severe and not enhanced by combination (Figs 2g and 3d, h and Supplementary Fig. 2k), both Ten-a and Ten-m probably

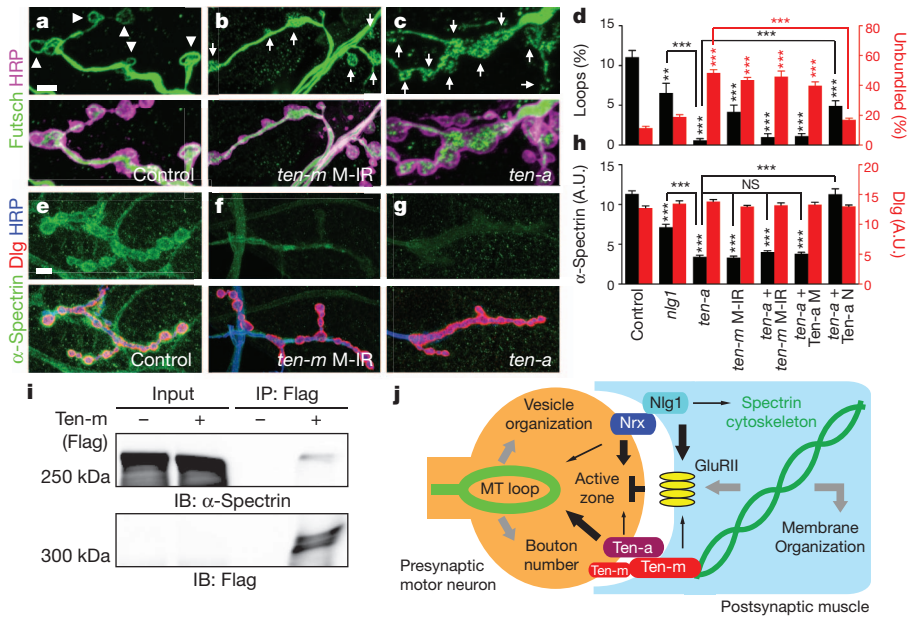

Figure 3 | Teneurin perturbation results in marked cytoskeletal disorganization. **a**–**c**, Representative NMJs stained with antibodies to Futsch (green) and HRP (magenta). Arrowheads indicate looped organization. Arrows indicate unbundled Futsch. **d**, Quantification of the percentage of total boutons with looped or unbundled microtubules. **e**–**g**, Representative NMJs stained with antibodies to α-Spectrin (green), Dlg (red) and HRP (blue). Following *teneurin* perturbation, α-Spectrin staining is largely lost. Axonal α-Spectrin is unaffected by muscle *teneurin* RNAi (**f**). **h**, Quantification of α-Spectrin (green) and Dlg (red) fluorescence. A.U., arbitrary units. For all genotypes, $n \geq 6$ larvae, 12 NMJs. **i**, Immunoblots (IB) showing that α-Spectrin is detected in the Flag immunoprecipitates (IP) of larvae expressing muscle Flag–HA-tagged Ten-m but not in control larvae. Owing to low expression, Flag–HA-Ten-m is only detectable after enrichment by immunoprecipitation. **j**, Model showing the roles of Teneurins, Neurexin and Neuroligin at the NMJ. Arrow size represents the relative contribution of each pathway to the cellular process as inferred from mutant phenotypic severity. Scale bars, 5 μm. ***$P < 0.001$, NS, not significant.

function in the same pathway. Our finding that Ten-a and Ten-m co-immunoprecipitate from different cells *in vitro*[8] and across the NMJ *in vivo* (Fig. 1f) further suggests a signal via a trans-synaptic complex. Teneurin function, however, may not be solely trans-synaptic. In some cases (vesicle density, SSR width), cell-autonomous knockdown resulted in stronger phenotypes than knocking down in synaptic partners (Supplementary Figs 3, 4, 9 and Supplementary Table 1). This suggests additional cell-autonomous roles in addition to trans-synaptic Teneurin signalling.

Signalling involving the transmembrane proteins Neurexin and Neuroligin also mediates synapse development[26]. In *Drosophila*, Neurexin (*nrx*) and Neuroligin 1 (*nlg1*) mutations cause phenotypes similar to *teneurin* perturbation: reductions in bouton number, active zone organization, transmission, and SSR width[27,28]. *nlg1* and *nrx* mutations do not enhance each other, suggesting that they function in the same pathway[28]. Consistently[27,28], we found that *nrx* and *nlg1* mutants exhibited largely similar phenotypes (data not shown). To investigate the relationship between the *teneurin* genes and *nrx* and *nlg1*, we focused on the *nlg1* null mutant. Both Nlg1 tagged with enhanced green fluorescent protein (Nlg1–eGFP) and endogenous Ten-m occupied a similar postsynaptic space (Supplementary Fig. 10a). *teneurin* and *nlg1* loss-of-function mutations also displayed similar bouton number reductions (Fig. 2e, g), vesicle disorganization (Supplementary Fig. 4), and ghost bouton frequencies (Supplementary Fig. 9). Other phenotypes showed notable differences in severity. In *nlg1* mutants, there was a 29% failure of active zone/glutamate receptor apposition (Fig. 2k and Supplementary Fig. 10d), compared to 15% for the strongest *teneurin* perturbation. The cytoskeleton of *nlg1* mutants, however, was only mildly impaired compared to that seen with *teneurin* perturbations (Fig. 3d, h and Supplementary Figs 6 and 7).

To examine further the interplay of *teneurin* and *nlg1*, we analysed *ten-a nlg1* double mutants. Both single mutants were viable, despite their synaptic defects. Double mutants, however, were larval lethal. We obtained rare escapers, which showed a 72% reduction in boutons, compared to a 50–55% decrease in single mutants (Fig. 2e). Active zone apposition in double mutants was enhanced synergistically over either single mutant (Fig. 2k and Supplementary Fig. 10e). Cytoskeletal defects in the double mutant resembled the *ten-a* mutant (Fig. 3 and Supplementary Figs 6 and 7). These data suggest that *teneurin* genes and *nrx* and *nlg1* act in partially overlapping pathways, cooperating to organize synapses properly, with Teneurins contributing more to cytoskeletal organization and Neurexin and Neuroligin to active zone apposition (Fig. 3j).

In the accompanying manuscript[8], we showed that although the basal Teneurins are broadly expressed in the *Drosophila* antennal lobe, elevated expression in select glomeruli mediates olfactory neuron partner matching. At the NMJ, this basal level mediates synapse organization. Analogous to the antennal lobe, we found elevated *ten-m* expression at muscles 3 and 8 using the *ten-m-GAL4* enhancer trap (Fig. 4a). We confirmed this for endogenous *ten-m*, and determined that it was contributed by elevated Ten-m expression in both nerves and muscles (Fig. 4b–g). Indeed, *ten-m-GAL4* was highly expressed in select motor neurons, including MN3-Ib, which innervates muscle 3 (ref. 29; Supplementary Fig. 11c). This elevated larval expression also varied along the anterior–posterior axis (Supplementary Fig. 12), and was specific for Ten-m, as Ten-a expression did not differ within or between segments (data not shown).

To test whether elevated Ten-m expression in muscle 3 and MN3-Ib affects neuromuscular connectivity, we expressed *ten-m* RNAi using *ten-m-GAL4*. Wild-type muscle 3 was almost always innervated (Fig. 4h). However, after *ten-m* knockdown, muscle 3 innervation failed in 11% of hemisegments (Fig. 4i, j). This required Ten-m on both sides of the synapse, as the targeting phenotype persisted following neuronal or muscle RNAi suppression using tissue-specific *GAL80* transgenes (Fig. 4j). *ten-a* RNAi did not show this phenotype (Fig. 4j), consistent with homophilic target selection via Ten-m. The phenotype

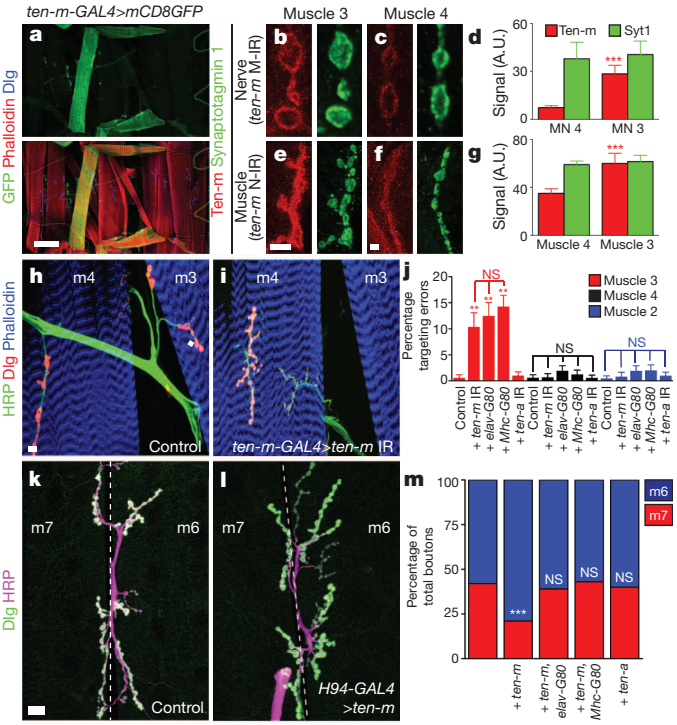

Figure 4 | High-level Ten-m expression regulates muscle target selection. **a**, Representative images of hemisegment A3 stained with antibodies to Dlg (blue), phalloidin (red), and expressing GFP via *ten-m-GAL4* (green). High-level expression is observed in muscles 3 and 8 and basally in all muscles. **b**, **c**, Muscle 3 (**b**) and 4 (**c**) NMJs show differential Ten-m (red) but similar Synaptotagmin 1 (Syt1; green) expression (from a *ten-m* muscle knockdown animal). **d**, Quantification of presynaptic Ten-m (red) and Syt1 (green) fluorescence at muscle 3 and 4 NMJs. MN, motor neuron. **e**, **f**, NMJs at muscles 3 (**e**) and 4 (**f**) show differential Ten-m (red) but similar Syt1 (green) expression in muscles (from a *ten-m* nerve knockdown). **g**, Quantification of postsynaptic Ten-m (red) and Syt1 (green) fluorescence at muscle 3 and 4 NMJs. **h**, **i**, Representative images stained with phalloidin (blue) and antibodies to HRP (green) and Dlg (red) to visualize motor neurons and muscles in control (**h**) or *ten-m-GAL4>ten-m* RNAi larvae (**i**). m, muscle. **j**, Quantification of the hemisegment percentage with failed muscle 3 (red), 4 (black) or 2 (blue) innervation. IR, interfering RNA. **k**, **l**, Representative images of the muscle 6/7 NMJ labelled with antibodies to Dlg (green) and HRP (magenta). The characteristic wild-type arrangement of boutons (**k**) is shifted towards muscle 6 when Ten-m is overexpressed in that muscle and the innervating motor neurons (**l**). **m**, Quantification of the total bouton percentage on muscles 6 (blue) and 7 (red). All genotypes contain *H94-GAL4*, additional transgenes are indicated (for details, see Methods). The Ten-m-mediated shift is abolished by neuronal or muscle *GAL80* transgenes. Scale bars, 100 μm (**a**), 5 μm (**b**–**i**), 10 μm (**k**, **l**). In all cases, $n \geq 12$ larvae. $^{***}P < 0.001$, $^{**}P < 0.01$, NS, not significant.

was specific to muscle 3, as innervation onto the immediately proximal or distal muscle was unchanged (Fig. 4j). The low penetrance is probably due to redundant target selection mechanisms[30]. Where innervation did occur, the terminal displayed similarly severe phenotypes to other NMJs (not shown). Thus, in addition to generally mediating synaptic organization, Ten-m also contributes to correct target selection at a specific NMJ.

To determine whether Ten-m overexpression could alter connectivity, we expressed Ten-m in muscle 6 (but not the adjacent muscle 7), and the motor neurons innervating both muscles using *H94-GAL4*. Normally, 60% of the boutons at muscles 6/7 are present on muscle 6 with 40% on muscle 7 (Fig. 4k, m). Ten-m overexpression caused a shift whereby 81% of boutons synapsed onto muscle 6 and only 19% onto muscle 7 (Fig. 4l, m). This shift also required both neuronal and muscle Ten-m, as neuronal or muscle GAL80 abrogated it (Fig. 4m). The effect was specific because Ten-a overexpression did not alter this synaptic balance (Fig. 4m), nor was it secondary to altered bouton

number, which was unchanged (data not shown). Therefore, elevated Ten-m on both sides of the NMJ can bias target choice. This, combined with evidence that Ten-m can mediate homophilic interaction *in vitro*[8], supports a trans-synaptic homophilic attraction model at the NMJ as in the olfactory system.

We identified a two-tier mechanism for Teneurin function in synapse development at the *Drosophila* NMJ. At the basal level, Teneurins are expressed at all synapses and engage in hetero- and homophilic bi-directional trans-synaptic signalling to organize synapses properly (Fig. 3j). Supporting this, Teneurins can mediate homo- and heterophilic interactions *in vitro*[8] and heterophilic interactions *in vivo* (Fig. 1f). At the synapse, Teneurins organize the cytoskeleton, interact with α-Spectrin, and enable proper adhesion and release site formation. Further, elevated Ten-m expression regulates target selection in specific motor neurons and muscles via homophilic matching and functions with additional molecules[30] to mediate precise neuromuscular connectivity. Teneurin-mediated target selection at the NMJ is analogous to its role in olfactory synaptic partner matching[8]. As Teneurins are expressed broadly throughout the antennal lobe, it remains an attractive possibility that they also regulate synapse organization in the central nervous system.

METHODS SUMMARY

Details of *Drosophila* stocks, immunostaining, electron microscopy, functional assays, construction of epitope-tagged Teneurin constructs, immunoprecipitation, imaging and statistical analysis can be found in Methods.

Full Methods and any associated references are available in the online version of the paper at www.nature.com/nature.

Received 14 June 2011; accepted 7 February 2012.
Published online 18 March 2012.

1. Williams, M. E., de Wit, J. & Ghosh, A. Molecular mechanisms of synaptic specificity in developing neural circuits. *Neuron* **68,** 9–18 (2010).
2. Giagtzoglou, N., Ly, C. V. & Bellen, H. J. Cell adhesion, the backbone of the synapse: ''vertebrate'' and ''invertebrate'' perspectives. *Cold Spring Harb. Perspect. Biol.* **1,** a003079 (2009).
3. Young, T. R. & Leamey, C. A. Teneurins: important regulators of neural circuitry. *Int. J. Biochem. Cell Biol.* **41,** 990–993 (2009).
4. Kenzelmann, D., Chiquet-Ehrismann, R., Leachman, N. T. & Tucker, R. P. Teneurin-1 is expressed in interconnected regions of the developing brain and is processed *in vivo*. *BMC Dev. Biol.* **8,** 30 (2008).
5. Li, H., Bishop, K. M. & O'Leary, D. D. Potential target genes of EMX2 include *Odz/Ten-M* and other gene families with implications for cortical patterning. *Mol. Cell. Neurosci.* **33,** 136–149 (2006).
6. Silva, J. P. *et al.* Latrophilin 1 and its endogenous ligand Lasso/teneurin-2 form a high-affinity transsynaptic receptor pair with signaling capabilities. *Proc. Natl Acad. Sci. USA* **108,** 12113–12118 (2011).
7. Leamey, C. A. *et al.* Ten_m3 regulates eye-specific patterning in the mammalian visual pathway and is required for binocular vision. *PLoS Biol.* **5,** e241 (2007) CrossRef.
8. Hong, W., Mosca, T. J. & Luo, L. Teneurins instruct synaptic partner matching in an olfactory map. *Nature* http://dx.doi.org/10.1038/nature10926 (this issue).
9. Liebl, F. L. *et al.* Genome-wide P-element screen for *Drosophila* synaptogenesis mutants. *J. Neurobiol.* **66,** 332–347 (2006).
10. Kurusu, M. *et al.* A screen of cell-surface molecules identifies leucine-rich repeat proteins as key mediators of synaptic target selection. *Neuron* **59,** 972–985 (2008).
11. Zheng, L. *et al. Drosophila* Ten-m and Filamin affect motor neuron growth cone guidance. *PLoS ONE* **6,** e22956 (2011).
12. Sone, M. *et al.* Synaptic development is controlled in the periactive zones of *Drosophila* synapses. *Development* **127,** 4157–4168 (2000).
13. Wagh, D. A. *et al.* Bruchpilot, a protein with homology to ELKS/CAST, is required for structural integrity and function of synaptic active zones in *Drosophila*. *Neuron* **49,** 833–844 (2006).
14. Potter, C. J., Tasic, B., Russler, E. V., Liang, L. & Luo, L. The Q system: a repressible binary system for transgene expression, lineage tracing, and mosaic analysis. *Cell* **141,** 536–548 (2010).
15. Marrus, S. B., Portman, S. L., Allen, M. J., Moffat, K. G. & DiAntonio, A. Differential localization of glutamate receptor subunits at the *Drosophila* neuromuscular junction. *J. Neurosci.* **24,** 1406–1415 (2004).
16. Wichmann, C. & Sigrist, S. J. The active zone T-bar—a plasticity module? *J. Neurogenet.* **24,** 133–145 (2010).
17. Aberle, H. *et al. wishful thinking* encodes a BMP type II receptor that regulates synaptic growth in *Drosophila*. *Neuron* **33,** 545–558 (2002).
18. Owald, D. *et al.* A Syd-1 homologue regulates pre- and postsynaptic maturation in *Drosophila*. *J. Cell Biol.* **188,** 565–579 (2010).
19. Kittel, R. J. *et al.* Bruchpilot promotes active zone assembly, Ca^{2+} channel clustering, and vesicle release. *Science* **312,** 1051–1054 (2006).
20. Roos, J., Hummel, T., Ng, N., Klambt, C. & Davis, G. W. *Drosophila* Futsch regulates synaptic microtubule organization and is necessary for synaptic growth. *Neuron* **26,** 371–382 (2000).
21. Pielage, J., Fetter, R. D. & Davis, G. W. A postsynaptic spectrin scaffold defines active zone size, spacing, and efficacy at the *Drosophila* neuromuscular junction. *J. Cell Biol.* **175,** 491–503 (2006).
22. Pielage, J., Bulat, V., Zuchero, J. B., Fetter, R. D. & Davis, G. W. Hts/Adducin controls synaptic elaboration and elimination. *Neuron* **69,** 1114–1131 (2011).
23. Mosca, T. J. & Schwarz, T. L. The nuclear import of Frizzled2-C by Importins-β11 and α2 promotes postsynaptic development. *Nature Neurosci.* **13,** 935–943 (2010).
24. Featherstone, D. E., Davis, W. S., Dubreuil, R. R. & Broadie, K. *Drosophila* α- and β-spectrin mutations disrupt presynaptic neurotransmitter release. *J. Neurosci.* **21,** 4215–4224 (2001).
25. Miech, C., Pauer, H. U., He, X. & Schwarz, T. L. Presynaptic local signaling by a canonical wingless pathway regulates development of the *Drosophila* neuromuscular junction. *J. Neurosci.* **28,** 10875–10884 (2008).
26. Craig, A. M. & Kang, Y. Neurexin–neuroligin signaling in synapse development. *Curr. Opin. Neurobiol.* **17,** 43–52 (2007).
27. Li, J., Ashley, J., Budnik, V. & Bhat, M. A. Crucial role of *Drosophila* Neurexin in proper active zone apposition to postsynaptic densities, synaptic growth, and synaptic transmission. *Neuron* **55,** 741–755 (2007).
28. Banovic, D. *et al. Drosophila* Neuroligin 1 promotes growth and postsynaptic differentiation at glutamatergic neuromuscular junctions. *Neuron* **66,** 724–738 (2010).
29. Landgraf, M., Roy, S., Prokop, A., VijayRaghavan, K. & Bate, M. *even-skipped* determines the dorsal growth of motor axons in *Drosophila*. *Neuron* **22,** 43–52 (1999).
30. Sanes, J. R. & Yamagata, M. Many paths to synaptic specificity. *Annu. Rev. Cell Dev. Biol.* **25,** 161–195 (2009).

Supplementary Information is linked to the online version of the paper at www.nature.com/nature.

Acknowledgements We thank H. Aberle, V. Budnik, A. DiAntonio, R. Dubreuil, D. Featherstone, N. Reist, T. Schwarz, S. Stowers, D. Van Vactor, R. Wides, the Bloomington Stock Center and the Developmental Studies Hybridoma Bank for fly stocks, antibodies and reagents; J. Perrino and D. Luginbuhl for technical assistance; K. Shen, K. Zinn, D. Banovic, D. Berns, Y. Chou, C. A. Frank, X. Gao, S. Hippenmeyer, K. Miyamichi, K. Sillar, B. Tasic, X. Yu and S. Zosimus for critiques. Supported by a National Institutes of Health (NIH) grant (R01 DC-005982 to L.L.), and Epilepsy, Neonatology and Developmental Biology Training Grants (NIH 5T32 NS007280 and HD007249 to T.J.M.). L.L. is an investigator of the Howard Hughes Medical Institute.

Author Contributions T.J.M. designed and performed all experiments (apart from electrophysiology). W.H. characterized and provided new reagents, and assisted in some experiments. V.S.D. and T.J.M. designed and V.S.D. performed electrophysiology experiments with assistance from T.J.M. V.F. provided new reagents. L.L. supervised the project. T.J.M. wrote the manuscript with feedback from all authors.

Author Information Reprints and permissions information is available at www.nature.com/reprints. The authors declare no competing financial interests. Readers are welcome to comment on the online version of this article at www.nature.com/nature. Correspondence and requests for materials should be addressed to T.J.M. (tmosca@stanford.edu).

METHODS

***Drosophila* stocks.** All *Drosophila* strains and controls were raised at 29 °C to maximize GAL4 expression. All mutants and transgenes were maintained over GFP balancer chromosomes to enable larval selection. *Mhc-GAL4* or *Mef2-GAL4* (ref. 31) was used to drive expression in all somatic muscles. *Nrv2-GAL4* (ref. 32) and *elav-GAL4* (ref. 33) were used to drive expression in all neurons. *H94-GAL4* was used to drive expression in muscles 6, 13 and 4 and their corresponding motor neurons[34]. *daughterless-GAL4* was used to drive expression ubiquitously[35]. *Synj-QF*[36] was used to drive expression in all nerves. *NP6658-GAL4* (*ten-m-GAL4*) was used to drive expression in the pattern of endogenous Ten-m expression[8]. The *Df(X)ten-a* deletion was used as a *ten-a* null mutant[8]. For *nlg1* mutants, the I960 and ex2.3 alleles were used in *trans*[28] and double mutant larvae with *ten-a* and *nlg1* mutations were obtained using optimized rearing conditions[37]. Because of the early lethality of the *ten-m* mutant[11], and to assess independently *ten-a*, tissue-specific RNAi was used to examine *teneurin* perturbation using the following RNAi transgenic strains: for *ten-m*, UAS-*ten-m*$^{RNAi\text{-}V51173}$ and for *ten-a* (ref. 8), *UAS-ten-a*$^{RNAi\text{-}V32482}$. The following transgenic strains were used: *UAS-Dcr2* (ref. 38), *UAS-Fas2* (ref. 34), *UAS-mCD8GFP* (ref. 39), *UAS-Nlg1-eGFP* (ref. 28), *UAS-Ten-a* (ref. 8), *P{GS}9267* for *ten-m* overexpression[8]. In all cases, the efficacy of RNAi transgenes, overexpression transgenes and the *ten-a* deletion mutant were assessed and verified by the alteration of antibody staining (loss, reduction or increase) using tissue-specific *GAL4* drivers. For all cases, N-IR indicates neuronal RNAi, M-IR indicates muscle RNAi, U-IR indicates ubiquitous RNAi. For rescuing *ten-a* mutants, Ten-a N indicates neuronal overexpression with *elav-GAL4* of *UAS-ten-a* and Ten-a M indicates muscle overexpression of *UAS-ten-a* with *Mef2-GAL4*.

Immunostaining. Wandering third instar larvae were processed as previously described[23]. The following primary antibodies were used: mouse antibody to Ten-m (mAb20, 1:500)[40], guinea pig antibody to Ten-a (1:100)[41], mouse antibody to Brp (mAbnc82, 1:250)[42], rabbit antibody to Synaptotagmin 1 (1:4,000)[43], mouse antibody to Cysteine String Protein (mAb6D6, 1:100)[44], mouse antibody to Dlg (mAb4F3, 1:500)[45], rabbit antibody to Dlg (1:40,000)[46], mouse antibody to α-Spectrin (mAb3A9, 1:50)[47], mouse antibody to Fasciclin 2 (mAb1D4, 1:20)[48], rabbit antibody to Fasciclin 2 (1:5,000)[46], mouse antibody to Futsch (mAb22C10, 1:50)[20], rabbit antibody to DGluRIII (1:2,500)[15], rat antibody to Elav (mAb7E8A10, 1:25)[49], mouse antibody to Even-skipped (mAb3C10, 1:100)[50], rabbit antibody to β-Spectrin (1:1,000)[51], mouse antibody to Hts (1:500)[22], guinea pig antibody to Wsp (1:1,000)[52]. Alexa488-, Alexa546- or Alexa647-conjugated secondary antibodies were used at 1:250 (Invitrogen). Texas-Red-conjugated Phalloidin was used at 1:300. FITC-, Cy3- or Cy5-conjugated antibodies to HRP were used at 1:100 (Jackson ImmunoResearch).

Electron microscopy. Wandering third instar larvae were processed and sectioned as described[23]. Sections were imaged on a JEM-1400 (JEOL) transmission electron microscope at ×3,000 to ×20,000 magnification.

Electrophysiology. Larvae were dissected in HL3 saline[53] containing 0 mM Ca^{2+} and 4 mM Mg^{2+}. They were then transferred to saline containing 0.6 mM Ca^{2+} and recordings conducted by impaling larval muscle 6 in body wall segments A3 and A4 using sharp intracellular electrodes (10–20 MΩ), fabricated from borosilicate glass capillaries and filled with 3 M KCl solution. For evoked EPSPs, severed nerve bundles were stimulated using a suction electrode connected to a linear stimulus isolated (A395, World Precision Instruments). Data, acquired using Multiclamp 700B amplifiers (Molecular Devices), were low-pass filtered at 3 kHz and digitized at 10 kHz. Recordings were acquired and analysed using Igor Pro software (Wavemetrics) and custom-written programs. All recordings in which the resting membrane potential was higher than −60 mV and/or whose resting potential, input resistance or access resistance changed by more than 20% during the duration of data acquisition were excluded from analysis. All recordings and data analyses were performed blind to the genotype. Quantal content was corrected for nonlinear summation[54].

Larval locomotion. Crawling assays were conducted as described[55].

FM1-43 dye loading. FM1-43 (Invitrogen) dye loading was conducted as described[56] with the following modifications: loading was conducted in 1.5 mM Ca^{2+}, 90 mM K^{+} saline for 1 min followed by six 2-min washes in 0 mM Ca^{2+} saline. Imaging was conducted on a Zeiss LSM 510 Meta Confocal (Carl Zeiss) with a ×40, PlanApo NA 1.0 water immersion lens (Carl Zeiss).

Construction of epitope-tagged teneurin transgenes. The *ten-m* and *ten-a* coding sequences lacking the stop codon were cloned into *pENTR-D/TOPO* (Invitrogen) from *pENTR-ten-m* and *pENTR-ten-a*[8]. *pENTR-ten-m(-stop)* and *pENTR-ten-a(-stop)* were recombined into the destination vectors *pUASTattB-gtw-tFHAH* and *pQUASTattB-gtw-tFMH*, respectively, using LR Clonase II (Invitrogen). pUASTattB-gtw-tFHAH is a pUASt-Gateway-attB based vector with a C-terminal TEV recognition site and 3×Flag, 3×HA and 10×His tags. *pQUASTattB-gtw-tFMH* is a *pQUASt-Gateway-attB*[8] based vector with a C-terminal TEV recognition site and 3×Flag, 6×Myc and 10×His tags. The resulting constructs were verified by restriction digest and sequencing and integrated into the *attP24* or *86Fb* landing sites on the second and third chromosomes[57]. Transgenic flies were verified by immunoprecipitation on western blot and overexpression experiments.

Immunoprecipitation, western blots and SDS–PAGE analysis. For Ten-m and Ten-a, *QUAS-Ten-a-Flag-Myc* was expressed in nerves using *Synj-QF* and *UAS-Ten-m-Flag-HA* in muscles using *mhc-GAL4*. Larval synaptosomes were prepared from larval body wall fillets as described[58]. For Ten-m and α-Spectrin, control larvae consisted of *Mef2-GAL4* without *UAS-Ten-m-Flag-HA* whereas experimental flies combined the two. Immunoprecipitation was conducted as described using M2-anti-Flag-conjugated agarose (Sigma) or Affi-Prep Protein A beads (Bio-Rad) and rat antibodies to HA (Roche)[23]. Proteins were separated on NuPAGE 3–8% Tris-Acetate Gels (Invitrogen) and transferred to nitrocellulose. Primary antibodies were applied overnight at 4 °C and secondary antibodies at 21 °C for 1 h. The following primary antibodies were used: mouse antibody to α-Spectrin (mAb3A9, 1:2,000), mouse antibody to Brp (mAbnc82, 1:100), mouse antibody to Flag (M2, 1:5,000, Sigma-Aldrich), mouse antibody to Myc (3E10, 1:1,500, Santa Cruz Biotechnology), rat antibody to HA (3F10, 1:1,500, Roche). HRP-conjugated secondary antibodies (Jackson ImmunoResearch) were used at 1:10,000. Blots were developed using the SuperSignal West Femto Maximum Sensitivity Substrate (ThermoScientific).

Imaging analysis. Larvae were imaged with a Zeiss LSM 510 Meta laser-scanning confocal microscope (Carl Zeiss) using either a ×63 1.4 NA or a ×40 1.0 NA objective. NMJ images were taken as confocal z-stacks with the upper and lower bounds defined by HRP staining unless otherwise noted. For all metrics, boutons were assessed in segment A3 at muscle 6/7 and muscle 4 on both the left and right sides. Fluorescence intensity measurements were taken from terminals on muscle 4. All phenotypes, however, were observed at all synapses regardless of muscle fibre or segment. For membrane organization, vesicle distribution and Teneurin colocalization, NMJ images were taken as single optical sections at the precise centre of the bouton as determined by HRP staining. Images were processed with the LSM software and Adobe Photoshop CS4. Bouton number, active zone/glutamate receptor apposition, fluorescent intensity and microtubule organization were quantified as previously described[23]. Targeting errors for each larva were quantified as the percentage of hemisegments from A1 to A7 in a single animal with a failure of target innervation. There was no difference in targeting errors based on body wall segment. Experiments using H94-GAL4 were conducted as described[34], and their effects confirmed using Fasciclin 2 overexpression (control = 58.1% of boutons on muscle 6, 41.9% on muscle 7; Fas 2 overexpression = 73.0% on muscle 6, 27.0% on muscle 7; $n = 8$ animals for each, $P < 0.0001$)[34].

In electron micrographs, parameters were quantified as previously described using ImageJ (NIH)[23]. T-bar defects were classified into one of five categories: normal (no discernible defect), double (two T-bars were observed in the same, continuous active zone), detached (where the T-bar was clearly visible but was not explicitly connected to the membrane associated with the nearest PSD), apposite contractile tissue (where the T-bar was not apposed to the SSR, but rather, the contractile tissue of the muscle), misshapen (where an electron-dense T-bar was visible but did not conform to the 'T' shape. Often, the T-bars were 'X' shaped). For Fig. 2r, each defect is expressed as a percentage of the total number of T-bars observed in a particular genotype.

For Ten-m gradient calculation, single optical sections were taken through the centre of the NMJ on muscle 3 or muscle 4, as determined by HRP immunoreactivity. The GFP signal (*ten-m-GAL4*) or antibody signal was then measured using ImageJ (NIH). For each larva, measurements were taken on the right and left sides of each indicated segment. The fluorescence for each segment was expressed as a percentage of the fluorescence from segment A1 in the same animal, on the same side of the larvae. For all larvae, segment A1 represented the maximal fluorescence.

Statistical analysis. Statistical analysis used GraphPad Prism 5 (Graphpad Software). In all cases involving more than two samples, significance was calculated using ANOVA followed by a Dunnett post-hoc test to the control sample and a Bonferroni post-hoc test among all samples. For two-sample cases, an unpaired Student's *t*-test was used to assess significance, unless otherwise indicated. In all cases, both methods provided similar significance measurements. In all figures, significance is with respect to control genotypes unless otherwise noted.

31. Lilly, B. *et al.* Requirement of MADS domain transcription factor D-MEF2 for muscle formation in *Drosophila*. *Science* **267,** 688–693 (1995).
32. Sun, B., Xu, P. & Salvaterra, P. M. Dynamic visualization of nervous system in live *Drosophila*. *Proc. Natl Acad. Sci. USA* **96,** 10438–10443 (1999).
33. Luo, L., Liao, Y. J., Jan, L. Y. & Jan, Y. N. Distinct morphogenetic functions of similar small GTPases: *Drosophila* Drac1 is involved in axonal outgrowth and myoblast fusion. *Genes Dev.* **8,** 1787–1802 (1994).
34. Davis, G. W. & Goodman, C. S. Synapse-specific control of synaptic efficacy at the terminals of a single neuron. *Nature* **392,** 82–86 (1998).

35. Wodarz, A., Hinz, U., Engelbert, M. & Knust, E. Expression of crumbs confers apical character on plasma membrane domains of ectodermal epithelia of *Drosophila*. *Cell* **82,** 67–76 (1995).
36. Petersen, L. K. & Stowers, R. S. A Gateway MultiSite recombination cloning toolkit. *PLoS ONE* **6,** e24531 (2011).
37. Loewen, C. A., Mackler, J. M. & Reist, N. E. *Drosophila synaptotagmin I* null mutants survive to early adulthood. *Genesis* **31,** 30–36 (2001).
38. Dietzl, G. *et al.* A genome-wide transgenic RNAi library for conditional gene inactivation in *Drosophila*. *Nature* **448,** 151–156 (2007).
39. Lee, T. & Luo, L. Mosaic analysis with a repressible cell marker for studies of gene function in neuronal morphogenesis. *Neuron* **22,** 451–461 (1999).
40. Levine, A. *et al. odd Oz*: a novel *Drosophila* pair rule gene. *Cell* **77,** 587–598 (1994).
41. Rakovitsky, N. *et al. Drosophila Ten-a* is a maternal pair-rule and patterning gene. *Mech. Dev.* **124,** 911–924 (2007).
42. Laissue, P. P. *et al.* Three-dimensional reconstruction of the antennal lobe in *Drosophila melanogaster*. *J. Comp. Neurol.* **405,** 543–552 (1999).
43. Mackler, J. M., Drummond, J. A., Loewen, C. A., Robinson, I. M. & Reist, N. E. The C_2B Ca^{2+}-binding motif of synaptotagmin is required for synaptic transmission *in vivo*. *Nature* **418,** 340–344 (2002).
44. Zinsmaier, K. E., Eberle, K. K., Buchner, E., Walter, N. & Benzer, S. Paralysis and early death in cysteine string protein mutants of *Drosophila*. *Science* **263,** 977–980 (1994).
45. Parnas, D., Haghighi, A. P., Fetter, R. D., Kim, S. W. & Goodman, C. S. Regulation of postsynaptic structure and protein localization by the Rho-type guanine nucleotide exchange factor dPix. *Neuron* **32,** 415–424 (2001).
46. Koh, Y. H., Popova, E., Thomas, U., Griffith, L. C. & Budnik, V. Regulation of DLG localization at synapses by CaMKII-dependent phosphorylation. *Cell* **98,** 353–363 (1999).
47. Byers, T. J., Dubreuil, R., Branton, D., Kiehart, D. P. & Goldstein, L. S. *Drosophila* spectrin. II. Conserved features of the alpha-subunit are revealed by analysis of cDNA clones and fusion proteins. *J. Cell Biol.* **105,** 2103–2110 (1987).
48. Van Vactor, D., Sink, H., Fambrough, D., Tsoo, R. & Goodman, C. S. Genes that control neuromuscular specificity in *Drosophila*. *Cell* **73,** 1137–1153 (1993).
49. O'Neill, E. M., Rebay, I., Tjian, R. & Rubin, G. M. The activities of two Ets-related transcription factors required for *Drosophila* eye development are modulated by the Ras/MAPK pathway. *Cell* **78,** 137–147 (1994).
50. Patel, N. H., Schafer, B., Goodman, C. S. & Holmgren, R. The role of segment polarity genes during *Drosophila* neurogenesis. *Genes Dev.* **3,** 890–904 (1989).
51. Byers, T. J., Husain-Chishti, A., Dubreuil, R. R., Branton, D. & Goldstein, L. S. Sequence similarity of the amino-terminal domain of *Drosophila* beta spectrin to alpha actinin and dystrophin. *J. Cell Biol.* **109,** 1633–1641 (1989).
52. Ben-Yaacov, S., Le Borgne, R., Abramson, I., Schweisguth, F. & Schejter, E. D. *Wasp*, the *Drosophila* Wiskott-Aldrich syndrome gene homologue, is required for cell fate decisions mediated by *Notch* signaling. *J. Cell Biol.* **152,** 1–13 (2001).
53. Stewart, B. A., Atwood, H. L., Renger, J. J., Wang, J. & Wu, C. F. Improved stability of *Drosophila* larval neuromuscular preparations in haemolymph-like physiological solutions. *J. Comp. Physiol. A Neuroethol. Sens. Neural Behav. Physiol.* **175,** 179–191 (1994).
54. Martin, A. R. A further study of the statistical composition on the end-plate potential. *J. Physiol. (Lond.)* **130,** 114–122 (1955).
55. Lnenicka, G. A., Spencer, G. M. & Keshishian, H. Effect of reduced impulse activity on the development of identified motor terminals in *Drosophila* larvae. *J. Neurobiol.* **54,** 337–345 (2003).
56. Verstreken, P., Ohyama, T. & Bellen, H. J. FM 1-43 labeling of synaptic vesicle pools at the *Drosophila* neuromuscular junction. *Methods Mol. Biol.* **440,** 349–369 (2008).
57. Markstein, M., Pitsouli, C., Villalta, C., Celniker, S. E. & Perrimon, N. Exploiting position effects and the gypsy retrovirus insulator to engineer precisely expressed transgenes. *Nature Genet.* **40,** 476–483 (2008).
58. Higashi-Kovtun, M. E., Mosca, T. J., Dickman, D. K., Meinertzhagen, I. A. & Schwarz, T. L. Importin-β11 regulates synaptic phosphorylated mothers against decapentaplegic, and thereby influences synaptic development and function at the Drosophila neuromuscular junction. *J. Neurosci.* **30,** 5253–5268 (2010).